J. Plasma Physics (2010), *vol.* 76, *parts* 3&4, *pp.* 655–664.
doi:10.1017/S0022377809990900

Cavity-hollow cathode-sputtering source for titanium films

R. SCHRITTWIESER[1], C. IONITA[1], A. MURAWSKI[1], C. MASZL[1], M. ASANDULESA[2], A. NASTUTA[2], G. RUSU[2], C. DOUAT[3], S. B. OLENICI[4], I. VOJVODIC[5], M. DOBROMIR[2], D. LUCA[2], S. JAKSCH[1] and P. SCHEIER[1]

[1] Institute for Ion Physics and Applied Physics, University of Innsbruck, Austria (Roman.Schrittwieser@uibk.ac.at)
[2] Faculty of Physics, Alexandru-Ioan-Cuza University of Iasi, Iasi, Romania
[3] UFR des Sciences, Université Paris Sud 11, Orsay Cedex, France
[4] ISAS – Institute for Analytical Sciences, Dortmund, Germany
[5] Faculty of Natural Sciences and Mathematics, University of Montenegro, Podgorica, Montenegro

Dedicated to the 60th birthday of Prof. Padma Kant Shukla, an extraordinary plasma physicist and a wonderful personality.

(Received 15 December 2009 and accepted 18 December 2009, first published online 22 January 2010)

Abstract. A cavity-hollow cathode was investigated as low-cost sputtering source for titanium. An argon discharge is produced inside a hollow cathode consisting of two specifically formed disks of titanium. An additional cavity further enhances the pendulum effect of the electrons. Measurements with small Langmuir probes yielded evidence for the formation of a space charge double layer above the cathode. The sputtered atoms form negatively charged clusters. After further acceleration by the double layer the clusters impinge on the substrates. Titanium thin films were produced on highly oriented pyrolytic graphite. The films were investigated by a scanning tunnel microscope and X-ray photoelectron spectroscopy.

1. Introduction

Thin film deposition is one of the most important technological applications of plasma physics. Various techniques are in use; among them are hollow cathodes (HC), which are simple and inexpensive. They do not need a magnetic field, which makes them particularly useful for sputtering of ferromagnetics. Hollow cathodes are used as intensive light sources [1], spectroscopic light sources [2], cluster sources [3], electron beam sources [4, 5], ion thrusters [6] and for deposition [7–10]. The most important part of an HC is its hollow cathode cylinder. The annular cathode fall acts as a deep potential well for the electrons, inside which they perform pendulum motion. This strongly enhances electron density, ionization and sputtering rate. The HC effect is known since long [11] (see also [12, 13]).

Often an additional cavity further enhances the effect. The cavity hollow cathode (CHC) creates a strong plasma jet at the muzzle of the hollow cathode. As a sputtering source, the CHC was first described in [14, 15]. The cathode is made of the material to be sputtered. The plasma ions are accelerated by the cathode

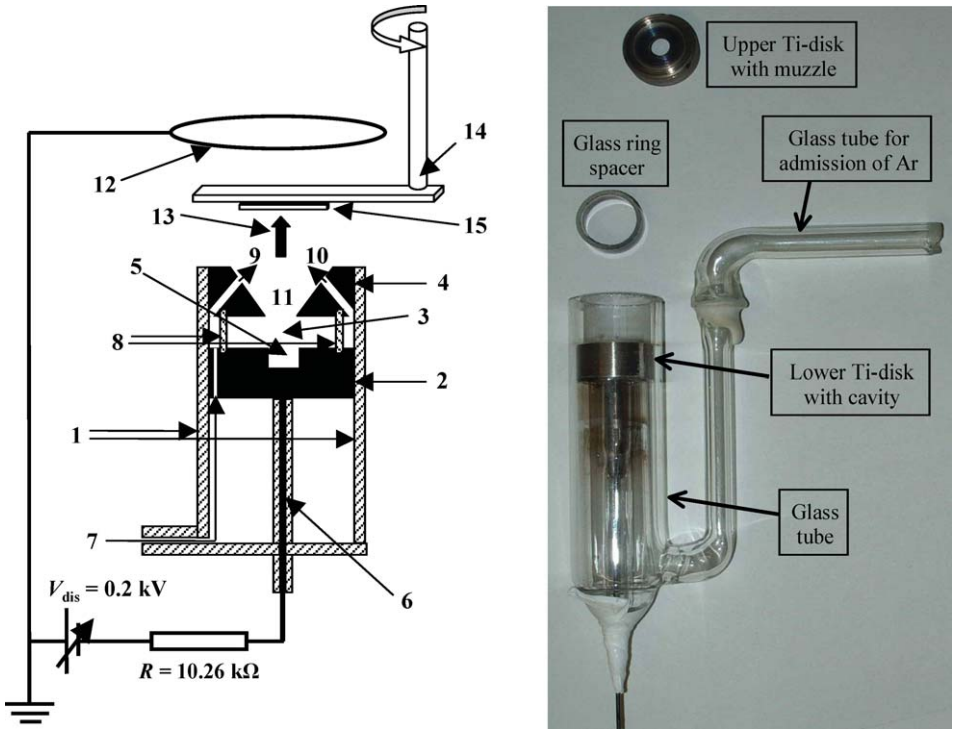

Figure 1. (Color online) (a) Schematic of the cavity hollow cathode (CHC) sputtering source. 1 glass tube, 2, 4 Ti-disks, 3 cathode chamber, 5 cathode cavity, 6 lead for biasing cathode, 7, 9, 10 gas channels, 8 glass ring spacer, 11 muzzle, 12 Cu-ring anode, 13 plasma jet, 14 pivoting substrate holder, also used as probe holder, 15 highly oriented pyrolytic graphite (HOPG) substrate. (b) Photo of the CHC, broken down into the main parts.

fall towards the cathode walls causing intensive sputtering. The sputtered particles are transported towards the substrate. The CHC was used to grow good quality thin films of TiN_xO_y, TiN, Ni and Fe [16–19]. The configuration was intensively investigated in dc and pulsed regimes [18, 20]. The film quality was enhanced by intense bombardment of the substrate by electrons. Inside the plasma jet, negatively charged clusters were found [3, 21]. Here, we concentrate on the discussion of probe measurements in the CHC plasma and the sputtering of titanium (Ti) thin films on highly oriented pyrolytic graphite (HOPG). The thin films were investigated by a scanning tunnelling microscope (STM) and X-ray photoelectron spectroscopy (XPS).

2. Experimental set-up and typical discharge data

A schematic presentation and photo of the CHC experiment is shown in Fig. 1. The CHC consists of two Ti disks with 18.3 mm outer diameter. The lower disk has a height of 9 mm (2). The upper disk is 7 mm high (4) and has a conical upward widening muzzle (11). The two disks are separated by a glass spacer (15 mm in diameter and 7 mm in height) (8), for optical measurements [18, 20]. Disks and glass spacer confine a 1.25 cm^3 cathode chamber (3). A cylindrical cavity (5 mm

https://doi.org/10.1017/S0022377809990900 Published online by Cambridge University Press

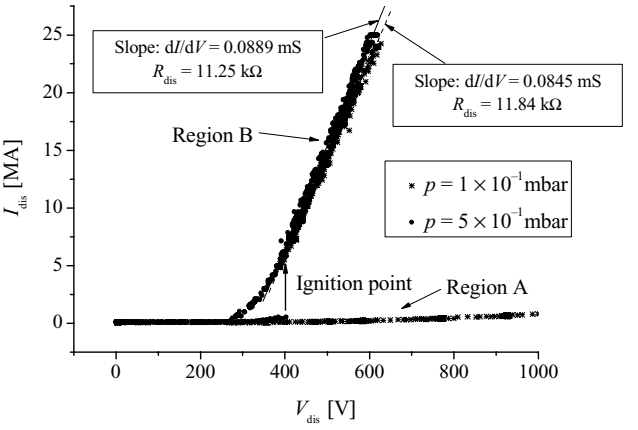

Figure 2. Current-voltage characteristic of the CHC for two different pressures as indicated in the figure. Region A indicates the glow discharge regime. Region B indicates the hollow cathode regime.

in diameter) (5) inside the lower disk further enhances ionization [14]. Both disks contain channels for the application of the operating gas argon (Ar) in front of the muzzle (7, 9, 10).

The cathode ensemble is introduced into a glass tube (Fig. 1(b) and 1 in Fig. 1(a)). The 5 litre stainless steel chamber (not shown in Fig. 1) acts as an anode. Sometimes a 30 mm diameter ring anode, 5 cm above the muzzle (12), was used as an anode. After about 1/2 h operation the glass spacer (8) becomes internally coated by the cathode material. This restricts the time for optical investigations and eventually connects the two cathode disks electrically, without altering the properties of the discharge. The substrate is pivoted into the space above the muzzle (11) by a holder (14), whose distance from the muzzle can be varied up to a few centimeters. Instead of the pivoting holder, Langmuir probes were inserted for electrical diagnosis of the plasma jet.

After evacuation to a base pressure of 10^{-3} Pa, Ar gas is applied in front of the muzzle through three inlets (7, 9 and 10 in Fig. 1(a)) up to pressures of 10–50 Pa. Typical current-voltage (I_{dis}-V_{dis}) characteristics of the CHC for two different pressures, namely 10 Pa and 50 Pa, are shown in Fig. 2; I_{dis} is the discharge current, and V_{dis} is the voltage applied to the CHC. Figure 3 shows photos into the muzzle. At low currents, a glow discharge is observed (Region A in Figs. 2 and 3(a)), created only outside the CHC between the upper disk and the anode. For a certain ignition voltage, the system suddenly jumps into the HC-discharge mode. This regime (Region B in Figs. 2 and 3(b)) is characterized by a dramatic increase of I_{dis}. The negative glow is confined inside the cavity and a conical plasma jet exits from the muzzle (Fig. 3(b)). For 10 Pa the ignition voltage is close to 1300 V, decreasing with increasing pressure to around 400 V for 50 Pa. The I_{dis}-V_{dis} characteristic shows a linear behaviour with its inverse slope representing the resistance of the discharge R_{dis} (Fig. 2).

The Ti thin films were investigated by means of an STM and XPS. The substrates were taken out from the CHC and inserted into the STM. Since the films were exposed to air, the Ti-layers were oxidized.

https://doi.org/10.1017/S0022377809990900 Published online by Cambridge University Press

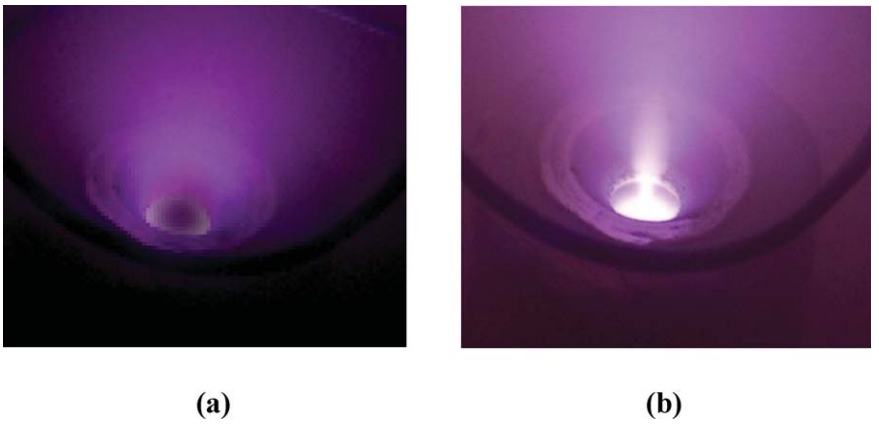

Figure 3. (Color online) The discharge above the CHC muzzle. (a) Glow discharge regime. (b) Hollow cathode regime.

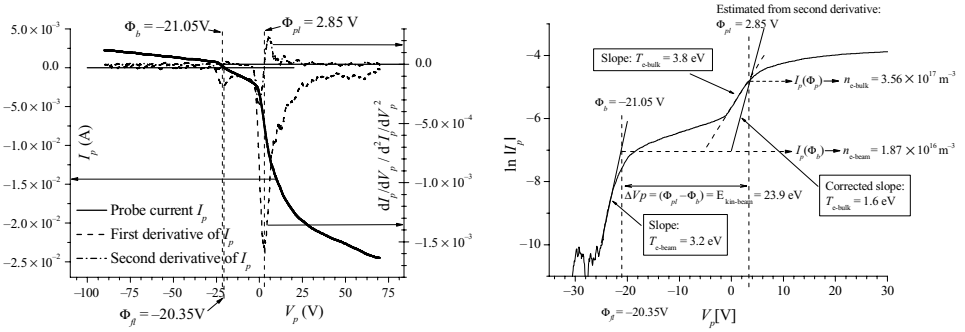

Figure 4. (a) $I_p - V_p$ characteristic (solid line and symbols) with its first (dashed line) and second (dashed-dotted line) derivative of the probe for $I_{\rm dis} = 20$ mA, pressure $p = 10$ Pa, 10 mm above cathode and on axis. The x-axis for the first (dashed line) and the second (dashed-dotted line) derivatives (right y-axis) is shifted slightly above the x-axis for the probe current (left y-axis). (b) Semi-logarithmic plot of electron current. See text for a detailed description of the figure.

3. Experimental results

3.1. Characterization of the hollow cathode regime by a Langmuir probe

Electrostatic measurements were performed with a small cylindrical tungsten wire, Langmuir probe (diameter 0.125 mm), above the CHC muzzle. The tip protrudes by 1 mm from the probe shaft, a ceramic tube (Al_2O_3) of 0.5 mm in diameter with a borehole of 0.2 mm diameter. Inside the tube the W-wire is tightly spliced on a length of about 20 mm with a certain number of very fine copper wires (threads) [22, 23]. The 0.5 mm ceramic tube is fixed by ceramic glue on a 1.2 mm ceramic tube. The electric connection of the probe wire (spliced Cu-threads) is connected to a vacuum feed-through.

The probe was swept from −70 V up to +70 V. The current-voltage ($I_p - V_p$) characteristics delivered the floating potential V_{fl}, plasma potential Φ_{pl}, electron temperature T_e and electron density n_e [24]. Figure 4(a) shows a typical characteristic of the probe inserted 10 mm above the muzzle on the axis. We see a

https://doi.org/10.1017/S0022377809990900 Published online by Cambridge University Press

complicated characteristic (black thick line – somewhat smoothed) with two bends, one at $V_p = -24.5$ V and the other at -1.5 V. The dashed line shows the first derivative of the smoothed characteristic, whereas the dashed-dotted line shows the second derivative. Applying Druyvesteyn's method, the second derivative should show the electron energy distribution (EED) [25]. However, as pointed out in [26], great care has to be taken with this method, especially in plasmas where the EED has no spherical symmetry, which obviously is not the case here. Druyvesteyn's method has also been critically reviewed in [27].

Therefore we assume the first derivative (dashed line in Fig. 4(a)) to indicate the probable form of the (negative) EED. Two maxima yield evidence for two electron populations: a large one with a maximum at $\Phi_{pl} = 2.85$ V and a smaller one with a maximum at $\Phi_b = -21.05$ V. Obviously, the large peak of the EED has to be interpreted as bulk plasma, whereas the small peak signifies an additional population of electrons with a mean kinetic energy $E_b \cong 23.9$ eV. This corresponds to the difference between the two peaks in the EED: $\Delta V_p = (\Phi_{pl} - \Phi_b) = E_b/e$. The latter population of the EED can be interpreted as electron beam, accelerated by a plasma double layer [28] with an approximate height of 24 V, situated at the muzzle of the CHC. Consequently, Φ_{pl} is the plasma potential at this position determined by the bulk electrons and ions. The beam electrons lead to additional ionization and thus help to sustain the DL.

After the subtraction of the ion saturation current, a semi-logarithmic plot of a current-voltage characteristic (Fig. 4(b)) yields a linear relation between $\ln |I_p|$ and V_p in the electron-retarding field region, provided the electrons possess a Maxwellian velocity distribution. Usually the electron temperature can be determined from the linear ascent of $\ln |I_p(V_p)|$. However, (Fig. 4(b)) shows two distinctly different ascents of the probe electron current with the probe voltage. Hence, the EED is clearly non-Maxwellian. Also, this indicates the presence of two groups of electrons with different energies and densities.

We can gain more information on the two electron populations as sketched in Fig. 4(b): The slopes of the two ascents yield a measure for the electron temperatures of the two electron populations. The first linear ascent (straight line) between about -25 and $-20\,V$ yields the electron temperature of beam electrons as $T_{\mathrm{e-beam}} \cong 3.2$ eV. The ascent of the main electron population between about 0 V and +5 V (straight dashed line) delivers at first an uncorrected temperature of around 3.8 eV. But for a precise determination of $T_{\mathrm{e-bulk}}$, the current carried by the beam electrons has to be subtracted. After this we can find a corrected value of the bulk electron temperature as $T_{\mathrm{e-bulk}} \cong 1.6$ eV.

By analogous procedure we derive approximate values for the beam and bulk electron densities as $n_{\mathrm{e-beam}} \cong 1.87 \times 10^{16}\mathrm{m}^{-3}$ and $n_{\mathrm{e-bulk}} \cong 3.56 \times 10^{17}\mathrm{m}^{-3}$, respectively. We use the intersection points of the tangents (solid line and dashed line) with the vertical lines at Φ_b and Φ_{pl}, respectively, as indications of the values of $\ln |I_p|$, from which we deduce the electron densities. Also, in this case the beam density has to be subtracted from the uncorrected value of the bulk electron density, but since $n_{\mathrm{e-beam}} \ll n_{\mathrm{e-bulk}}$, the correction is very small.

3.2. Results of Ti thin film sputtering

Figure 5 shows a typical spectrum of the CHC discharge, taken through the glass ring spacer (near 8 in Fig. 1(a)), before it got too strongly coated to get reliable

https://doi.org/10.1017/S0022377809990900 Published online by Cambridge University Press

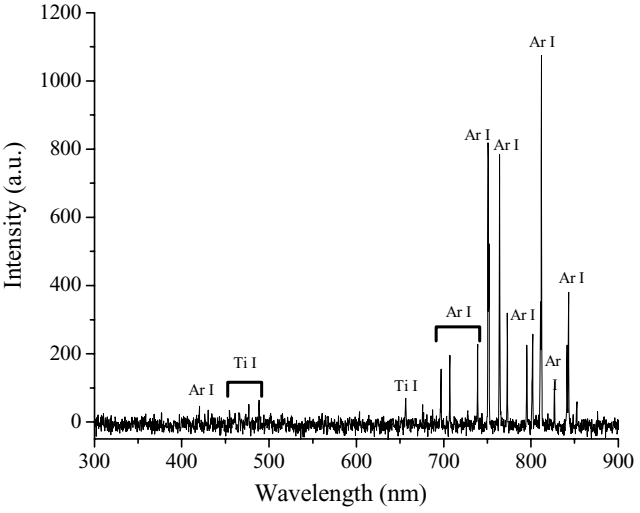

Figure 5. Typical spectrum of the CHC discharge with Ti disks as cathodes and Ar as working gas.

results. We see a number of Ar I and Ti I lines, but no ion lines and no traces of impurities.

The HOPG substrates were exposed to the plasma jet (containing Ti clusters) for two different durations of 30 s and 5 s at a distance, $d = 10$ mm, in front of the muzzle of the upper disk. The discharge current was 20 mA and the gas pressure 20 Pa. After that the coated HOPG substrate was removed from the CHC and brought to the STM for investigations [29].

Figures 6(a) and (b) show examples of the scanning by the STM over an area of 500×500 nm. Finer grains are found in the sample with the shorter exposure time (Fig. 6(b)). Figure 6(a) shows a thin white line along which a sectional scan of the thin film roughness was made (Fig. 7(c)). From the distance between two minima (as indicated by two downward arrowheads) the diameter of the grains was determined to be between 8 nm and 12 nm. This result corroborates the presumption that the Ti grains consist of rather large clusters, since the atomic radius of Ti is only about 0.18 nm. In case of Fig. 6(b) the grains had a typical size of 4–6 nm.

Figure 8(a) shows the results of a nano-lithography carried out by means of the STM. In this case, the tunnelling current was increased for three runs from the usual value of 20 pA to values between 2 nA and 3 nA, respectively. This leads to an evaporation of most of the Ti grains in the topmost layer of clusters so that a pit is formed and the lower layers of Ti grains become visible. The central white line in Fig. 8(a) shows the trace of the sectional thickness scan shown in Fig. 8(b). Thereby the depth of the hole was determined as approximately 0.6 nm (indicated by two downward arrowheads). This is much less than the diameter of the grains of 8–12 nm in the horizontal plane, so we find a discrepancy between the horizontal and vertical dimensions of the clusters. This is also the case for the finer grains in Fig. 6(b).

We have to take into account that even slight traces of oxygen in the residual vacuum suffice to oxidize the Ti surface [30], so that what we actually see is a surface of titanium oxide (TiO_2). Figure 7 shows an XPS spectrum of a Ti thin

https://doi.org/10.1017/S0022377809990900 Published online by Cambridge University Press

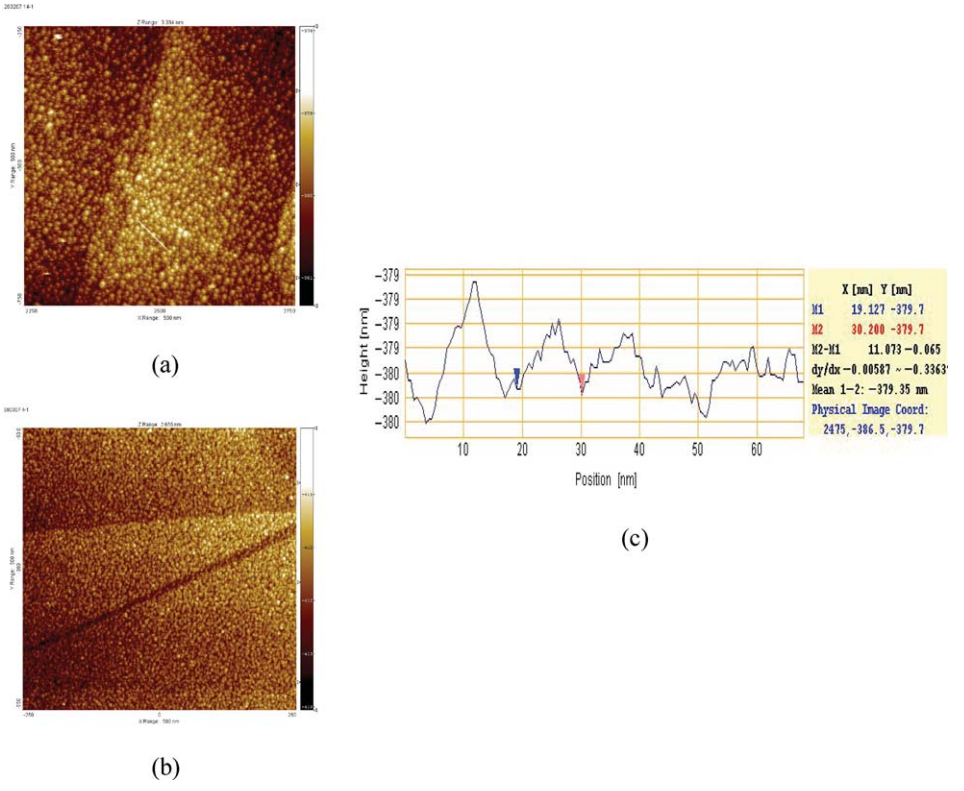

Figure 6. (Color online) Examples of STM scans of Ti thin films on HOPG, area of 500 × 500 nm, Ar-pressure 20 Pa, discharge current 20 mA and 10 mm above the muzzle. (a) 30 s exposure time with scanning parameters of 2.3 V and 10 pA. (b) HOPG 5 s exposure time with scanning parameters of 2.3 V and 20 pA. (c) Sectional scan along the white line in (a).

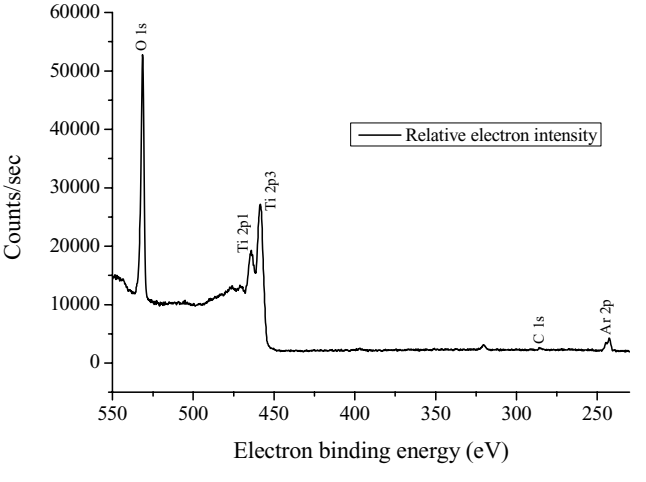

Figure 7. XPS spectrum of a Ti thin film created by the CHC discharge with Ti disks as cathodes and Ar as working gas.

https://doi.org/10.1017/S0022377809990900 Published online by Cambridge University Press

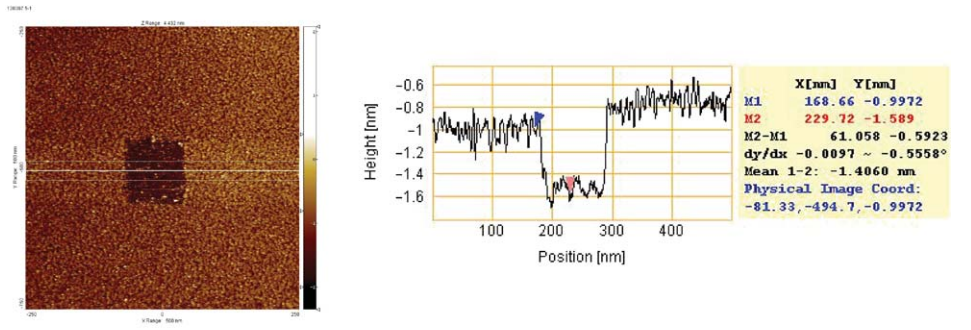

(a) (b)

Figure 8. (Color online) (a) Ti thin film deposited with similar parameters as in Fig. 6 (HOPG exposed for 15 s) after nano-lithography of a hole by means of the STM. Scanning parameters 2.3 V and 20 pA, with the hole of 100 × 100 nm created by a tunnelling current of 2–3 nA with a gap voltage of 2.3 V. (b) Corresponding averaged sectional scan along the white line.

film. In addition to the two Ti-peaks there is a strong oxygen peak, which is a clear indication that the Ti thin film was oxidized, as remarked above. There is a trace of Ar gas due to the formation of the thin film in Ar plasma.

4. Discussion

4.1. Probe measurements

We have found an evidence for an electron beam above the muzzle of the CHC [16, 18, 31] with an energy of about 24 eV (see Fig. 4(a)). We assume that this beam is created by a plasma double layer [28]. Double layers often appear in plasmas with strong electron currents, especially at sudden variations of the diameter of the current channel, where the current density changes [32]. Thus, it also seems plausible that the widening of the channel of the CHC in the muzzle gives rise to the formation of a double layer. Comprehensive investigations of the plasma in the CHC muzzle and in the jet above it with Langmuir probes (see Sec. 3.1.) substantiate this assumption (see also [33]). The plasma potential inside the CHC should have a value corresponding to the first small peak of the EED, *i.e.* $\Phi_b \cong -21.05$ V approximately.

4.2. Surface investigations

In the electric field of double layer, other negative charge carriers can also be accelerated towards the substrate in addition to the effect of the pressure gradient in this region. As we have found evidence for the formation of Ti clusters in the plasma jet, which, as usually, become negatively charged, these can also be accelerated by the double layer towards the substrate. This additional kinetic energy could contribute to a compression of the originally spherical clusters after an impact on the substrate and deliver a partial explanation for the oblate form of the Ti grains after deposition as discussed above.

Nevertheless, the discrepancy between the measured diameter of about 8–12 nm of the Ti grains parallel to the substrate plane (Fig. 8) and their measured height of less than 1 nm (Fig. 7) is not yet fully understood. Another reason could be that the density of states of the lithographically treated film is increased, so most of the height change would be compensated by this discrepancy of the local density of states (LDOS). Also, the tip of the STM was not calibrated in the z-direction.

https://doi.org/10.1017/S0022377809990900 Published online by Cambridge University Press

5. Conclusion

By using a CHC-sputtering source, we have obtained high-quality thin films of Ti on HOPG. The HC regime of the discharge was investigated by a Langmuir probe and evidence for the formation of a plasma double layer was found in the region above the muzzle of the CHC, which produces an electron beam in addition to the bulk electrons.

The high sputtering rate of the Ti cathodes is provided by the HC pendulum effect of the electrons. The sputtered Ti atoms gather in the form of clusters, which are negatively charged in the plasma jet exiting from the CHC muzzle. The thin films were investigated by means of STM and XPS. From an STM scan we have obtained an estimate of the cluster size as 8–12 nm. These negatively charged clusters are accelerated together with the electrons towards the grounded substrate, impinging there with a higher kinetic energy after being accelerated through the double layer.

Acknowledgements

The first two authors would like to express their gratitude to Prof. Padma K. Shukla for his constant encouragement. This work was supported by the Romanian Ministry of Education and Research, the Austrian Science Fund (through FWF-Projects P14545-PHY and L302-N02), the CEEPUS II network AT-0063, the Socrates-Erasmus programme and the European Commission (through the FP6-I3 project ITS-LEIF).

References

[1] Sullivan, J. V. and Walsh, A. 1965 *Spectrochimica Acta* **21**, 721–726.

[2] Baude, S., Broekaert, J. A. C., Delfosse, D., Jakubowski, N., Fuechtjohann, L., Orellana-Velado, N. G., Pereiro, R. and Sanz-Medel, A. 2000 *J. Anal. At. Spectrom.* **15**, 1516–1525.

[3] Xenoulis, A. C., Doukellis, G., Tsouris, P., Karydas, A., Potiriadis, C., Katsanos, A. A. and Tsakalakos, Th. 1998 *Vacuum* **51**, 357–362.

[4] Burdovitsin, V. A. and Oks, E. M. 2008 *Laser Particle Beams* **26**, 619–635.

[5] Gu, X., Meng, L., Yan, Y. and Sun, Y. 2009 *J. Infrared Milli. Terahz. Waves* **30**, 1083–1091.

[6] Fearn, D. G. 1978 *J. Spacecraft Rockets* **15**, 154–161.

[7] Gavrilov, N., Mesyats, G., Radkovski, G. and Bersenev, V. 1997 *Surf. Coat. Technol.* **96**, 81–88.

[8] Ishii, K., Amano, K. and Hamakake, H. 1999 *J. Vac. Sci. Technol.* A **17**, 310–313.

[9] Oks, E. M., Anders, A. and Brown, I. G. 2004 *Rev. Sci. Instrum.* **75**, 1030–1033.

[10] Hubička, Z. et al. 2008 *Contrib. Plasma Phys.* **48**, 515–520.

[11] Pahl, M., Howorka, F., Märk, T. D., Lindinger, W. and Helm, H. 1973 *Acta Phys. Austriaca* **37**, 101–121.

[12] Bardos, L. 1996 *Surf. Coat. Techn.* **86–87**, 648–656.

[13] Zhechev, D., Zhemenik, V. I., Tileva, S., Mishinsky, G. V. and Pyrvanova, N. 2003 *Nucl. Instr. Method. Phys. Res.* B **204**, 387–391.

[14] Kazemeini, M. H., Berezin, A. A. and Fukuhara, N. 2000 *Thin Solid Films* **372**, 70–77.

[15] Kazemeini, M. H. and Berezin, A. A. 2000 *J Vacuum Sci. Techn.* A **18**, 2908–2913.

[16] Balan, P. C., Apetrei, R., Luca, D., Ionita, C., Schrittwieser, R. and Popa, G. 2005 *J. Optoel. Adv. Mater.* **7**, 2459–2464.

[17] Guruvenket, S. and Rao, G. M. 2002 *J. Vac. Sci. Technol.* A **20**, 678–682.

[18] Apetrei, R., Alexandroaei, D., Luca, D., Balan, P., Ionita, C., Schrittwieser, R. and Popa, G. 2006 *Jpn. J. Appl. Phys.* **45**, 8128–8131.

[19] Luca, D. 1996 *Rom. Reports in Phys.* **47**, 768–796.

[20] Apetrei, R., Alexandroaei, D., Luca, D., Balan, P., Ionita, C., Schrittwieser, R. and Popa, G. 2006 *Jpn. J. Appl. Phys.* **45**, 8132–8135.

[21] Qing Ma and Rosenberg R. A. 1999 *Phys. Rev.* B **60**, 2827–2832.

[22] Siebenförcher, A. and Schrittwieser, R. 1996 *Rev. Sci. Instrum.* **67**, 849–850.

[23] Schrittwieser, R., Ionita, C., Balan, P. C., Cabral, J. A., Figueiredo, H. F. C., Pohoata, V. and Varandas, C. 2001 *Contrib. Plasma Phys.* **41**, 494–503.

[24] Huddelstone, R. H. and Leonard, S. L. 1965 *Plasma Diagnostic Techniques*. New York, London: Academic Press.

[25] Druyvesteyn, M. J. 1930 *Z. Phys.* **64**, 781–798.

[26] Allen, J. A. 1978 *J. Phys.* D: *Appl. Phys.* **11**, L35–L36.

[27] Popov, T. K., Dimitrova, M., Dias, F. M., Tsaneva, V. N., Stelmashenko, N. A., Blamire, M. G. and Barber, Z. H. 2006 *J. Phys.: Conf. Series* **44**, 60–69.

[28] R. Schrittwieser (Ed.) 1993 *Proc. of Fourth Symp. on Double Layers and Other Nonlinear Potential Structures in Plasmas* (Innsbruck, Austria, 1992). Singapore: World Scientific Publishing Company, p. 498.

[29] Vojvodic, I., Olenici, S. B., Ionita, C., Jaksch, S., Balan, P., Rasul, B., Scheier, P. and Schrittwieser, R. 2007 Titanium thin films sputtered by a cavity hollow cathode discharge on highly oriented pyrolytic graphite In: *Proc. XXVIIIth Int. Conf. Phenomena in Ionized Gases* (eds. J. Schmidt, M. Simek, S. Pekarek and V. Prukner). Prague, Czech Republic, pp. 657–660.

[30] Linsmeier, C., private communication.

[31] Schrittwieser, R., Ionita, C., Luca, D., Alexandroaei, D., Apetrei, R., Anita, V., Popa, G., Balan, P. C., Olenici, S. B. and Murawski, A. 2007 In: *16th Symp. Appl. Plasma Proc.—SAPP 2007. Inv. Lect. IL10*, *Book of Abstracts*, Podbanské, Slovakia, pp. 75–78.

[32] Langmuir, I. 1929 *Phys. Rev.* **33**, 954–989.

[33] Murawski, A. 2006 Characterization of a cavity-hollow cathode as a sputter source for various materials. *Master's Thesis*, University of Innsbruck, Austria.